Experimental investigation on the effects of shoreface nourishment placement and timing on long-term cross-shore profile development

Larsen, Bjarke Eltard; van der A., Dominic A.; Carstensen, Rex; Carstensen, Stefan; Fuhrman, David R.

Published in:
Coastal Engineering

Link to article, DOI:
10.1016/j.coastaleng.2022.104258

Publication date:
2023

Document Version
Publisher's PDF, also known as Version of record

Coastal Engineering 180 (2023) 104258

Contents lists available at ScienceDirect

Coastal Engineering

journal homepage: www.elsevier.com/locate/coastaleng

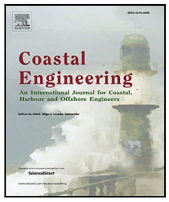

Experimental investigation on the effects of shoreface nourishment placement and timing on long-term cross-shore profile development

Bjarke Eltard Larsen [a,*], Dominic A. van der A [b], Rex Carstensen [a], Stefan Carstensen [a], David R. Fuhrman [a]

[a] Technical University of Denmark, Department of Civil and Mechanical Engineering, DK-2800, Kgs. Lyngby, Denmark
[b] School of Engineering, University of Aberdeen, Aberdeen, AB24 3UE, United Kingdom

ARTICLE INFO

Dataset link: 10.11583/DTU.16739449

Keywords:
Nourishment
Experiments
Equilibrium profile
Bar migration

ABSTRACT

Experimental results involving shoreface nourishment scenarios are presented. The experiments are performed at small scale and the effects of nourishment placement and timing in relation to long-term cross-shore profile development are investigated. Four different nourishment scenarios are tested experimentally, with nourishment positioned both in the trough of a pre-developed profile as well as along the bar of the profile. The results demonstrate that under all scenarios the erosion of the shoreline slows relative to the case without nourishment. The two cases where the nourishment was placed along the bar reduced erosion of the shoreline more compared to the two cases with nourishment in the trough onshore of the bar. Compared to past experiments on nourishment presented in the literature, the present experiments were run for a longer duration, and the concepts of equilibrium profile and the development towards such an equilibrium were investigated. Curiously, the experiments showed a reversal of the sediment transport rate from being primarily offshore directed across the entire profile to onshore directed in the inner surf zone region closest to the shoreline. This reversal of transport rate occurred without changing the incoming wave conditions and resulted in deposition at the shoreline. This either questions the existence of equilibrium beach profiles or at the very least shows that the development towards such an equilibrium will not always be monotonic in time.

1. Introduction

Sand nourishment is often used as coastal protection as it has fewer negative side effects compared to hard structures (Dean, 2002). Nourishments can be deployed either in the form of a beach nourishment (on the emerged part of the beach profile and the swash region) or a shoreface nourishment (on the submerged part of the profile), also called profile nourishment by Dean (2002). When positioned at the shoreface (typically either in the trough of a breaker bar or along the bar slope and crest), a nourishment can potentially protect the beach by acting as a feeder mechanism. Additionally, shoreface nourishment can force irregular waves to break earlier and/or more frequently, thereby reducing the amount of wave energy that hits the beach (a sheltering effect). In nourishment research there has often been a tendency to completely separate the longshore and cross-shore effects (Dean, 2002). According to Dean (2002), this is done both because the cross-shore developments are often seen to occur over much shorter time scales than those in the longshore direction, and, perhaps more importantly, for practical reasons. Models that work well for predicting longshore sediment transport are still not very accurate for predicting cross-shore sediment transport, and even specific cross-shore models struggle with accurately predicting cross-shore processes without site specific calibration (van Rijn et al., 2011; Ruessink et al., 2012; Dubarbier et al., 2015).

There have been many field measurements on the effect of shoreface nourishments (see e.g van Duin et al., 2004; Grunnet and Ruessink, 2005; Huisman et al., 2019). These have provided valuable insights, but they are still rather case specific. Furthermore, due to the inherent complexity of field conditions, differences between cross-shore and longshore effects could not be separated. As such, isolating cross-shore effects on shoreface profile nourishments requires either numerical or experimental modelling.

There are very few detailed experimental nourishment papers. Walstra et al. (2010) used a small scale flume to study the effects of shoreface nourishments in both erosive and accretive conditions. They concluded that placing sand in the trough of the breaker bar reduced erosion of the upper profile (from approximately mid surf zone to

* Corresponding author.
E-mail address: bjelt@dtu.dk (B.E. Larsen).

https://doi.org/10.1016/j.coastaleng.2022.104258
Received 5 October 2021; Received in revised form 7 November 2022; Accepted 26 November 2022
Available online 2 December 2022

maximum run-up) more than the case where the nourishment was positioned on the bar. The duration of the experiments was not long enough to see an effect of shoreface nourishment placement strategy on the shoreline. Grasso et al. (2011) similarly studied shoreface nourishments as well as beach nourishments in a small scale flume using light weight (plastic) sediments. Their experiments simulated a storm with initially increasingly energetic waves followed by less energetic waves. Grasso et al. (2011) concluded that nourishments placed at the beach face were more efficient than the shoreface nourishments placed at the bar crest or the bar trough. For the shoreface nourishments no clear distinction could be made between cases where the nourishment was placed in the bar trough or on the bar crest. Di Risio et al. (2010) considered beach nourishments in conjunction with a submerged breakwater and concluded that the combination of a submerged breakwater with beach nourishment was more efficient in protecting the beach compared to beach nourishment alone. Recently, Atkinson and Baldock (2020) looked at nourishments in relation to sea-level rise. They considered beach nourishments, shoreline nourishments, and what they called surf zone nourishments (shoreface nourishment of the bar trough) and concluded that a nourishment placed in the surf-zone was most efficient in limiting recession of the entire profile, whereas nourishment placed at the upper beach was most efficient in limiting recession of the shoreline as it prevented wave over-topping.

The relative scarcity of experimental studies makes it difficult to understand the processes and nourishment strategies from a pure cross-shore perspective, and there remain differing opinions on where in the cross-shore profile the nourished sand should be placed. van Rijn et al. (2011) stated that nourishment is most efficient when placed shorewards of the innermost bar crest and that troughs should always be filled, which is similar to the findings by Walstra et al. (2010). This was not supported by Grasso et al.'s (2011) experiments, however, which showed little difference between nourishing the bar crest or the trough. It is also in contrast to the numerical simulations by Jacobsen and Fredsøe (2014), which showed that placing nourishing sand in the trough led to greater loss of sand than nourishment placed at the bar.

Following Dean's (2002) overall ideas on cross-shore processes, it seems evident that a single optimal nourishment strategy may not exist. According to Dean (2002) beaches are expected to revert to an equilibrium profile determined by the grain size and wave climate alone, which will happen over a relatively short time frame. Therefore, any sand placed on the shoreface will be beneficial as it will shift the entire profile seawards, but in the long term there will (in pure cross-shore terms) not be any difference in the profiles based on where the sand is placed. This line of thought has led to several methods which can predict an equilibrium profile's response to nourishment (see e.g. Rosati et al., 2013; Atkinson et al., 2018)

While the concept of an equilibrium profile is appealing it does not necessarily hold. Field measurements show that equilibrium profile shape is not reached immediately following nourishments, which indicates that nourishment strategies might have an impact (at least in the medium term). van Duin et al. (2004) reported that nourishing sand placed offshore of the crest of the outer bar caused the bar to grow and migrate in the onshore direction; only after 2 years did the system start to revert to its natural state (with a slow offshore migration of the outer bar). For a similar double barred profile (Ojeda et al., 2008) also demonstrated onshore migration of the shoreface nourishment, as well as slowing of the natural offshore migration of the two breaker bars. This is, as Huisman et al. (2019) states in relation to the presented field measurements, because placing a shoreface nourishment likely disturbs the cross-shore sediment transport balance.

In this study we wish to investigate the following research questions: (1) Is the long-term cross-shore profile development affected by adding a nourishment? (2) Does placement and timing of the nourishment material affect the long-term nature of the profile development? These questions will be addressed by systematically investigating cross-shore nourishment placement and timing under controlled laboratory conditions, with the long-term development of an unnourished profile subject to the same wave climate serving as a control case. Please note that the questions posed above clearly limit our investigation to cross-shore processes. These research questions are relevant to coastal engineering, as it is often assumed that cross-shore processes will matter little, and that the cross-shore profile will revert quickly towards its long-term equilibrium (see e.g. Dean, 2002). Indeed the results presented in the paper shows that this assumptions may need to be revisited. We investigate the effect of timing as longshore breaker bars are not fixed and tend to migrate. This can happen over several years in a cyclic fashion, on a slightly shorter time frame between winter and summer seasons, or even on a very short (daily) time frame, due to a storm. Additionally, this paper will also shed light on cross-shore sediment transport and morphology in general, as well as the very notion of equilibrium profiles. Finally, the dataset of the present experiments is made available open source, which can be very valuable for model validation.

As the experiments in the present study are performed at model scale (with associated scaling issues), we stress that the present experiments should not be viewed as a direct model scale version of specific nourishment field cases, and that conclusions made regarding the direction of cross-shore sediment transport rates from the present experiments may not necessarily be immediately transferred to the field. Rather this study presents a more fundamental study on the effect of nourishment material on long-term cross-shore profile development.

2. Experimental set-up, procedure, scaling and data treatment

The present experiments were conducted in a 28 m long, 0.8 m deep and 0.6 m wide wave flume at the Technical University of Denmark (DTU), which was fitted with a piston type wave maker with active wave absorption. At a distance of 12.5 m from the wave paddle a constant fixed slope $S = 1/25$ was installed, and initially a 15 cm layer of well-sorted sand was added on top of the slope. The sand had a median grain diameter $d_{50} = 0.18$ mm, with an estimated fall velocity $w_s = 0.0173$ m/s based on the method of Fredsøe and Deigaard (1992). Throughout the experiments the water depth offshore of the sloping region was kept constant at $h = 0.5$ m. Along the length of the flume 10 resistance type wave gauges were installed to measure the surface elevations. Five of the wave gauges were positioned in the flat part of the flume and the remaining five wave gauges were placed with approximately 1.5 meter intervals along the sloping bed. Fig. 1 shows a sketch of the initial experimental setup as well as the positions of the wave gauges along the length of the flume. Included in the figure (solid red line) is also the expected equilibrium profile based on Bruun (1954) and Dean (1991, 2002):

$$h(\chi) = A\chi^{2/3}, \tag{1}$$

where χ is the offshore distance from the shoreline and A is a proportionality constant, which was fitted on a case-to-case basis by Bruun (1954), while Dean (1991, 2002) obtained the following grain/fall velocity dependent parameter in

$$A = 0.067 w_s^{0.44} \tag{2}$$

with w_s expressed in cm/s. As can be seen from Fig. 1 the chosen slope matches the predicted profile well. The x-origin of the coordinate system is at the wave paddle, and the z-origin is at the still water level.

Along the length of the flume three video cameras were placed to monitor wave breaking and the inner surf zone. Not all wave series were recorded and the field-of-view of each camera was changed from wave series to wave series. These recordings were used to quantify the predominant wave breaker type and observe the evolution of the breaking bore.

A single downward looking Omron ZX1-LD600 laser distance meter, mounted on a trolley on the top of the flume, was used to track the

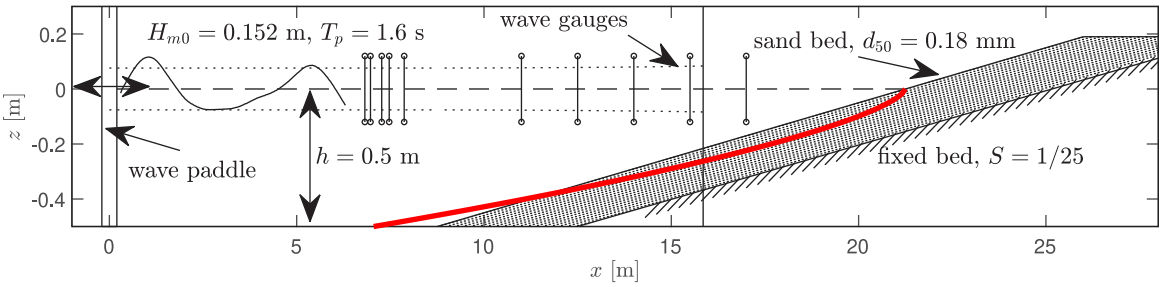

Fig. 1. Experimental setup. Included are also the predicted surface elevation maxima and minima using linear theory (dotted lines) and a breaking criterion of $H_s/h = 0.77$ (vertical solid line) as well as the 2/3-power profile predicted following (1) (red line).

vertical position of the bed. The position of the trolley was measured by a horizontal looking SICK DT50-2 laser distance meter mounted at the beach end of the flume. The vertical laser distance meter had an accuracy of ±0.5 mm and the horizontal laser distance meter an accuracy of ±5 mm. At selected times the bed was profiled using the vertical and horizontal laser distance meters. The bed was generally scanned in two sequences: First the water level was lowered to $h \approx 0.3$ m and the dry part of the profile was scanned. Subsequently the water level was slowly raised to $h \approx 0.75$ m and the bed was scanned with the encased sensor submerged. The combined submerged and emerged scan constitutes the entire bed scan. Great care was taken when filling and draining the flume to avoid disturbing the profile.

All cases had the same wave conditions throughout the experiments. The target spectrum (repeating itself every half hour) was a JONSWAP spectrum with a peak enhancement factor $\gamma = 3.3$, a significant wave height (at the paddle) $H_s = 0.15$ m and peak wave period $T_p = 1.6$ s. The average measured $H_s \approx H_{m0} = 4\eta_{std}$ across all the runs at the five wave gauges in the flat part of the flume was $H_{m0} = 0.152$ m, where η is the water surface elevation and η_{std} is the standard deviation of the surface elevation. These conditions correspond to $k_p h = 1.02$ and deep water wave steepness $H_{\infty,m0}/L_{\infty,m0} = 0.041$ where k_p is the peak wave number and $H_{\infty,m0}$ and $L_{\infty,m0}$ are deep water wave height and wave length respectively, calculated from linear wave theory using H_{m0}. We stress that utilizing a fixed wave climate over such long duration without water level variations is not representative of realistic field scale conditions. This was purposely done to be able isolate the effect of nourishment strategies on the natural un-nourished profile development over long duration.

The initial 1/25 bed slope was subjected to waves for 125 h thereby reaching a single barred profile in a state close to "equilibrium" as will be shown later. This un-nourished case will be used as a reference case for comparison against the different nourishment scenarios. During the 125 h the bed was frequently scanned, and two of these instants ($t = 40$ h and $t = 75$ h) were chosen as initial conditions for the nourishment cases. These times were chosen as the respective profiles were significantly different from both the initial constant slope and the final measured profile and also from each other. For the nourishment cases, the bed was manually restored to the profile at the chosen time and then subjected to an additional 15 h of waves before the nourishment was applied. This was done to allow for the formation of bed forms and to compact the sand bed again after it was loosened as result of the manual restoration. This 15 h run between reshaping and the nourishment also allowed for testing the repeatability of the experiments, which is important for comparing the different cases against each other and against the reference case. After each nourishment scenario, before the bed was restored to its next initial condition, the added sand was removed to ensure having the same amount of sand in the flume as in the un-nourished case.

The nourishment in the experiments, using the same sand as the in profile, was added either in the trough of the breaker bar or in a thin long layer at the crest of the bar and along the offshore slope of the bar. Both types of nourishment placements have been used in nourishment projects in the field (van Duin et al., 2004). The different cases are summarized in Table 1. Where case Ref is the un-nourished reference case and cases starting with capital letter P are un-nourished cases following restoration. In these cases the subsequent two numbers in the case name indicate the starting time of the run, the next two numbers the end time of the run and the last number after the underscore is a counter. Cases staring with capital letter T are trough nourishment cases with the number indicating the time (in h) of the nourishment. Similarly, cases with capital letter B are bar nourishment cases, again with the number indicating the timing of the nourishment. Fig. 2 shows an example of both a trough nourishment (case T75) and bar nourishment (case B75), with the nourishing sand shaded in green.

Table 1
Details of the experiments. Overview of naming, initial conditions, start times (T_{start}), end times (T_{end}) and nourishment volume ($V_{nourishment}$) of the different cases in the present experimental campaign. All cases had $H_{m0} = 0.152$ m, $T_p = 1.6$ s and a $h = 0.5$ m in the constant depth region near the wave paddle.

Case	Initial condition	T_{start} [h]	T_{end} [h]	$V_{nourishment}$ [m^3/m]
Ref	1/25 slope	0	125	–
P2540_1	Profile	25	40	–
P2540_2	Profile	25	40	–
P6075_1	Profile	60	75	–
P6075_2	Profile	60	75	–
T40	Trough nourishment	40	145	0.30
B40	Bar nourishment	40	206	0.30
T75	Trough nourishment	75	145	0.30
B75	Bar nourishment	75	145	0.30

The compacted volume of nourishment was 0.30 m^3/m for all cases. This experimental nourishment volume is in line with Grasso et al. (2011), who applied approximately 0.3 m^3/m in a similar size flume. The volume of the present experiments is also similar to Walstra et al. (2010), who used approximately 0.25 m^3/m in a similar size flume. In all cases the nourishment was placed loosely on the bed and manually levelled to maintain span wise uniformity.

2.1. Scaling

The present experiments were performed at model scale and consequently scale effects were inevitably present. Therefore, it is not the aim of the present work to represent one specific field case or set of cases, but instead we aim to investigate more generically how placement and timing of nourishment can affect the morphological development towards an equilibrium profile. Nevertheless, it is still necessary to consider and discuss the possible scaling effects.

As the experiments used sediment grains with similar size as in typical field conditions, the settling velocity will be too high compared to the field, which impacts the morphology; beaches tend to be steeper in model scale compared to field scale as described by Vellinga (1982) and recently discussed in detail by Bayle et al. (2021). It should be noted though that, even if the sediment grain size was scaled, the settling velocity would still not follow Froude scaling (due to a Reynolds number dependency of the drag coefficient of sand), and the grain size

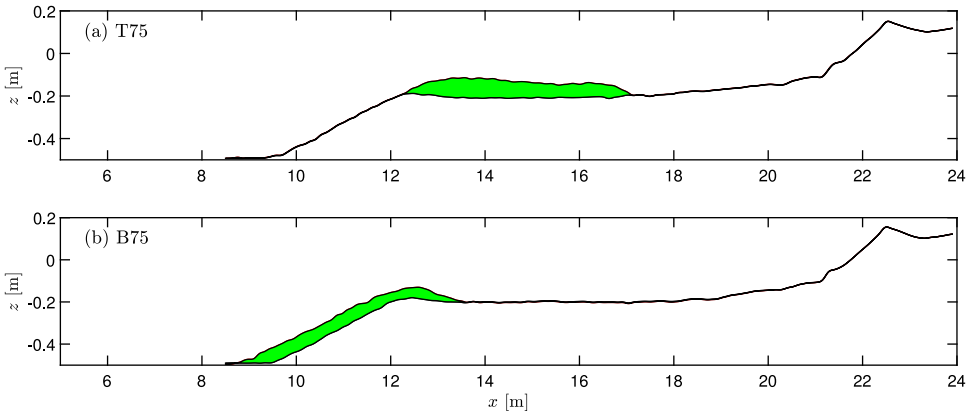

Fig. 2. Example of (a) trough nourishment (case T75) and (b) bar nourishment (case B75) with the green area showing the nourishment material.

could get close to the cohesive range. Additionally, the choice of grain size means that the Shields parameter

$$\theta = \frac{U_f^2}{g(s-1)d} \tag{3}$$

is not similar between model and field scale. Here U_f is the friction velocity, $g = 9.81\,\mathrm{m/s^2}$ is gravitational acceleration and $s = 2.65$ is the relative density of sand with respect to water. The difference in Shields parameter between model and field scale has implications for the mode of transport, which will be bed load dominated at model scale, and consist of both bed load transport and suspended transport at field scale.

The dissimilarity in Shields parameters between model and field scale also resulted in bed ripples forming in the experiments, spanning from the shoaling region (prior to breaking) through most of the surf zone, which would not be expected in the field. In the swash zone no ripples were present. Ripples can affect the direction of the sediment transport rate such that different grain sizes can travel in different directions under similar wave conditions and e.g. change the sign from onshore to offshore directed transport in the shoaling region (see e.g. van der A et al., 2013).

While not expecting full similarity with the field scale equivalents, it is still important to reconcile with important non-dimensional numbers normally used to describe cross-shore wave, sediment transport and morphological processes. The experimental conditions yield a Gourlay number (Gourlay, 1968 often referred to as the Dean number as will also be done for the remainder of this article):

$$\Omega = \frac{H_{\infty,m0}}{w_s T_p} \tag{4}$$

of $\Omega = 6.0$ This number can be used to classify beach profile types (Wright and Short, 1984). Wright and Short (1984) used an alternative Dean number based on wave height at breaking, H_b,

$$\Omega_b = \frac{H_b}{w_s T_p}. \tag{5}$$

According to Wright and Short (1984) beaches with $\Omega_b \leq 1$ will mostly be reflective beaches which are steep and dominated by surging breakers. Beaches with $\Omega_b \geq 6$ are alternatively characterized as dissipative beaches (also sometimes referred to as storm profiles) with mild slopes and spilling breakers. Beaches with $1 < \Omega_b < 6$ are characterized as intermediate state beaches, often consisting of pronounced bars and a mixture of plunging and spilling breakers. In the present study $\Omega_b = 6.0$ using linear wave theory and a breaking criterion of $H_s/h = 0.77$, which indicates that the chosen model beach profile is in the intermediate to dissipative range (note that the similarity between the two Dean numbers is due to the similarity between $H_{\infty,m0} = 0.166\,\mathrm{m}$ and the predicted wave height at breaking, $H_b = 0.167\,\mathrm{m}$)

Also of importance is the surf similarity parameter, ξ_∞.

$$\xi_\infty = \frac{S}{\sqrt{H_{\infty,m0}/L_{\infty,m0}}}. \tag{6}$$

Using the initial slope $S = 1/25$ yields $\xi_\infty = 0.2$, which indicates predominantly spilling breakers based on the classification by Galvin (1968), which was confirmed visually in the lab and through video analysis. During the course of the experiments the slope on the offshore side of the bar increased such that $\xi_\infty \approx 0.55$ at the end of the experiments. This indicates a shift towards more plunging breakers, which was also confirmed visually in lab as well as by video analysis.

2.2. Water surface elevations and sediment transport rates

In addition to presenting results from the bed scans, the present paper will also present parameters derived from the water surface elevation measurements. In this paper the characteristic wave heights have been calculated as

$$H_{m0} = 4\eta_{std}. \tag{7}$$

Also of importance is the wave skewness, which is a measure for the ratio between crest and trough heights and is calculated as

$$Sk(\eta) = \frac{\langle \eta^3 \rangle}{\eta_{std}^3}, \tag{8}$$

where the angular brackets represents time-averaging. We also consider the wave asymmetry, which is a measure for the ratio between water surface steepness at the wave front versus the wave rear and is defined as (Elgar and Guza, 1985)

$$As(\eta) = \frac{\langle \mathcal{H}(\eta)^3 \rangle}{\eta_{std}^3}. \tag{9}$$

Here, $\mathcal{H}$ is the Hilbert transform. For sawtooth-shaped waves with a steep front and mild rear slope, $As(\eta)$ is negative. Wave skewness and wave asymmetry are both very important for the cross-shore sediment transport rates (see e.g. van der A et al., 2013)

The total sediment transport rate between two instants in time can be estimated from the measured bed profiles using the discrete Exner equation

$$q_T(x) = q_T(x - \Delta x) + \Delta x(1-n)\frac{\Delta z_{bed}(x)}{\Delta t}, \tag{10}$$

here q_T is the volumetric sediment transport rate, Δx is horizontal discretization of the bed profile measurements, $\Delta z_{bed}(x)$ is the vertical difference between two bed measurements at location x, Δt is the time between the two bed scans and $n = 0.4$ is the porosity. Eq. (10) can be solved assuming zero transport from either the right (onshore) or left (offshore) side. The results from both sides will not yield exactly the same result, but will follow the same trend, with transport rate simply

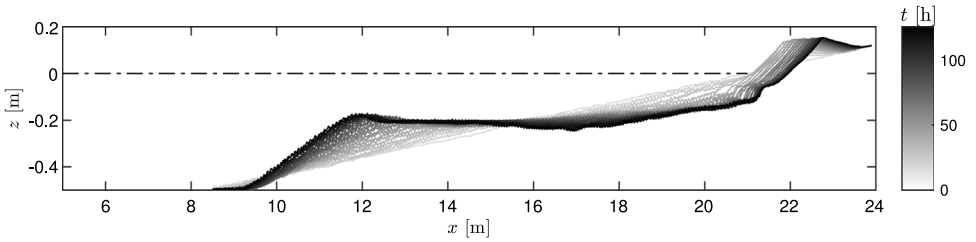

Fig. 3. Morphologic development Ref from t = 0–125 h. Light colours represent early scan and dark colours represent the latest scans.

shifted positively or negatively. This shift can be due to differences in bed compaction, or slight non-uniformity of the profile in the spanwise direction. Although these differences are small, they can cause a shift in the transport rate curves. Following the approach by van der Zanden et al. (2017) the transport rates are considered most accurate close to each of the horizontal boundaries, and therefore the total transport rate has generally been calculated as a weighted average between each end according to

$$q_T = \frac{x_{end} - x}{x_{end} - x_0} q_{lhs}(x) + \frac{x - x_0}{x_{end} - x} q_{rhs}(x) \tag{11}$$

where x_0 = 8.5 m is the left-hand boundary (the limit of the extent of the trolley), x_{end} = 23.9 m is the right-hand boundary, and q_{lhs} and q_{rhs} are the transport rates calculated from the left and right side respectively. Towards the end of case B40, the toe of the bar slope moved in the offshore direction beyond x_0 (see forthcoming Figs. 9 and 13), indicating that there was no longer zero transport here. For these conditions the transport rate was calculated based on q_{rhs} only.

3. Results and discussion

3.1. Reference case and repeatability

Fig. 3 shows all the bed profile measurements from the reference case (Ref) with light colours representing the earliest scans and dark colours the latest scans. All subsequent scans of the reference case are taken with a time interval of 5 h. From the initial constant slope, it can be seen that the bar evolves around $x \approx$ 14–15 m and slowly grows and migrates offshore with time. Shoreward of the shoreline a berm is formed, which can be seen to migrate onshore and grow in height.

During the entire 125 h duration of the experiment the shoreline retreated a total of approximately 0.9 m. For the first 25 h the shoreline position was almost constant, however, the beach was steepening during this time. Fig. 4 shows the temporal variation of the shoreline position x_{shore}, the horizontal position of the crest of the bar x_{bar}, the water depth at the crest of the bar h_{bar}, the horizontal berm position x_{berm} and the height of the berm h_{berm}. The crest of the bar is here defined as the offshore position where the deposition is largest relative to the initial profile and the horizontal position of the berm is similarly defined as the onshore position where the deposition is largest relative to the initial profile. The berm height is defined as the absolute height relative to the still water level. Bar movement, berm movement and shoreline movement were fastest initially and slowed with time as the profile developed towards an apparent equilibrium. Fig. 4 indicates that the reference case is close to being in equilibrium after 125 h; the shoreline position, bar position and berm position are almost constant, and both the depth at the breaker bar and the height of the berm appear to have reached an equilibrium. The development shown in Fig. 4 reveals a typical monotonic development towards equilibrium, in accordance with simple shoreline models (see e.g. Yates et al., 2009) i.e. the morphological development is fastest initially when the profile is in strongest dis-equilibrium.

Fig. 5 shows the bed profile, characteristic wave height, wave skewness, wave asymmetry and sediment transport rates at three selected times: at the start ($t \approx$ 2.5 h, black lines and symbols), in the middle ($t \approx$ 60 h, green lines and symbols) and towards the end of the experiments ($t \approx$ 125 h, red lines and symbols). Please note that the timing for the sediment transport rates is given as an approximate as these are calculated based on the profiles at t = 0 h and t = 5 h. At $t \approx$ 2.5 h (black lines and symbols) the characteristic wave heights (Fig. 5b) are almost constant in the flat part of the flume and on the slope until $x \approx$ 14 m, after which H_{m0} gradually declines indicating the position of the main break point. Both the wave skewness (Fig. 5c) and the asymmetry (Fig. 5d) are nearly constant in the flat part of the flume

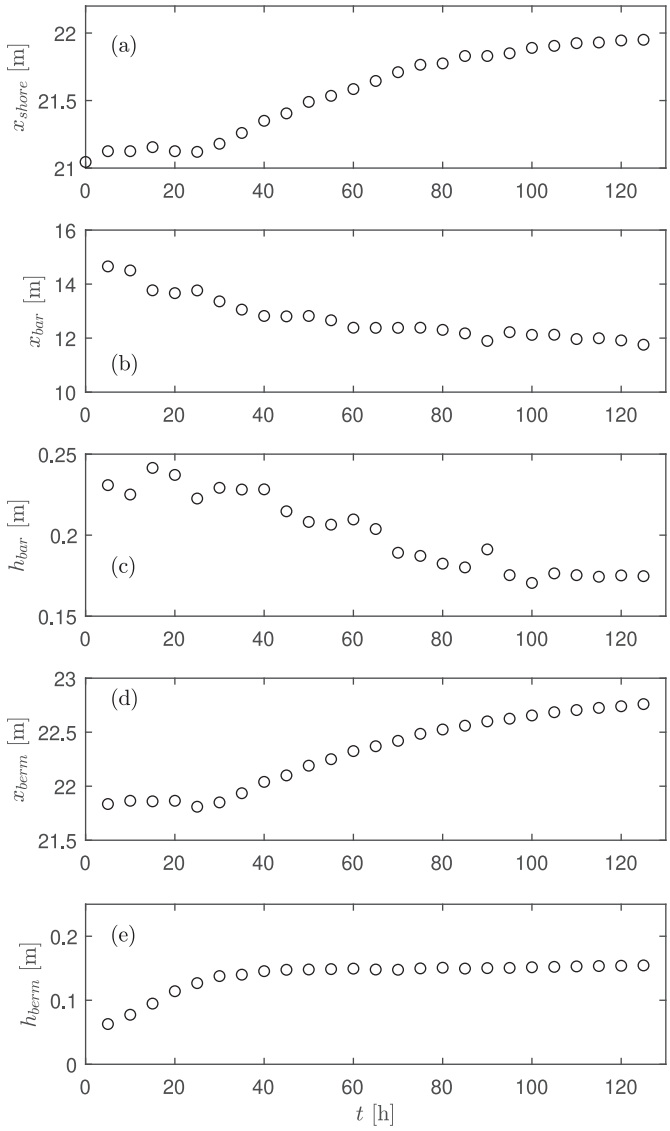

Fig. 4. Development of (a) shoreline position, (b) breaker bar position, (c) breaker bar water depth, (d) berm position and (e) berm height.

and increase in magnitude on the slope. The resulting initial sediment transport rates (Fig. 5e) can be described by three different regions. On the initial part of the slope the transport rate is onshore as is often seen in shoaling regions. This is followed by a long region with offshore directed sediment transport, with a peak in magnitude around $x \approx 15$ m, which is quite close to the break point. This is expected as the undertow is normally strongest near the break point (see e.g. van der A et al., 2017) and the amount of sediment in suspension is also highest near the break point (see e.g. van der Zanden et al., 2016). That the amount of sediment in suspension was highest near the break point was confirmed visually in the laboratory. In the very inner surf zone and the swash zone ($x > 19$ m), the transport rate is again onshore directed. This onshore directed transport is responsible for an initial steeping of the beach, and explains why the shoreline did not retreat for the first 25 h, as previously mentioned. As the bar is formed and moves offshore at $t \approx 60$ h, Fig. 5b (green symbols) shows that the waves break earlier, as expected, and the decline in characteristic wave height is stronger. The magnitude of both the skewness and asymmetry do not continue to grow throughout the surf zone, instead the skewness levels off at $Sk(\eta) \approx 1$ and the magnitude of the asymmetry reaches a maximum before declining again in the inner surf zone. The sediment transport rate at this time is offshore directed across the entire profile (green dotted lines in Fig. 5e), with the exception of a very small region onshore of the shoreline, which is responsible for moving the berm in the onshore direction as demonstrated in Fig. 4. The now offshore-directed sediment transport rate across the entire shoaling region may be explained by the increased steepness of the offshore slope, which promotes gravity driven offshore transport, and the presence of ripples, which under skewed waves may lead to wave-driven offshore transport. Inside the surf zone the offshore directed sediment transport rate is almost constant, indicating that there is not much profile change in this region. At $t \approx 125$ h the waves break even further offshore and skewness and asymmetry magnitudes both peak at $x \approx 12.5$ m, after which they decline, reaching almost the same levels in the inner surf zone as the offshore incoming waves (red crosses in Fig. 5b,c,d). The resulting sediment transport rate is still offshore directed in the shoaling region and in most of the surf zone, but at $x > 16$ m the transport rate changes sign, now becoming onshore directed. This could indicate that sand has started returning to the beach and that some of the lost shoreline would be recovered. The experiments were stopped at this point, however, to allow time for the nourishment cases. Despite not continuing all the way to equilibrium (if such a static equilibrium exists, see discussion in Section 4) the duration of this reference case and the following nourishment cases were still substantially longer than what is normally considered in the literature involving experimental nourishments (see e.g. Di Risio et al., 2010; Walstra et al., 2010; Grasso et al., 2011 who ran their cases 19 h, 24 h and 10 h respectively).

The reason for the change in sign of the sediment transport rate at $t \approx 122.5$ h is believed to be related to cessation of wave breaking in the inner surf zone. It was visually observed that at the end of the experiment very few broken waves remained as breakers all the way to the shore, i.e. the waves breaking at the breaker bar transformed into non-breaking waves. This is also indicated by the wave skewness and asymmetry, which, in the inner surf zone have almost the same value as the offshore incoming waves. The reformed non-breaking waves subsequently shoal again and break/collapse close to the shoreline, leading to onshore sediment transport in the upper profile and swash zone. This onshore-directed sediment transport at the foreshore after the secondary wave breaking may be due to the onshore wave-driven transport dominating the offshore directed undertow-related transport. The positive correlation between the onshore orbital flow and turbulence (see e.g. Ting and Kirby, 1994; Christensen et al., 2019) and the front–back wave asymmetry will lead to onshore wave-driven transport, whereas the undertow and hence the associated offshore-directed transport is expected to be weak due to the low wave heights. The onshore directed sediment transport in the inner surf zone and

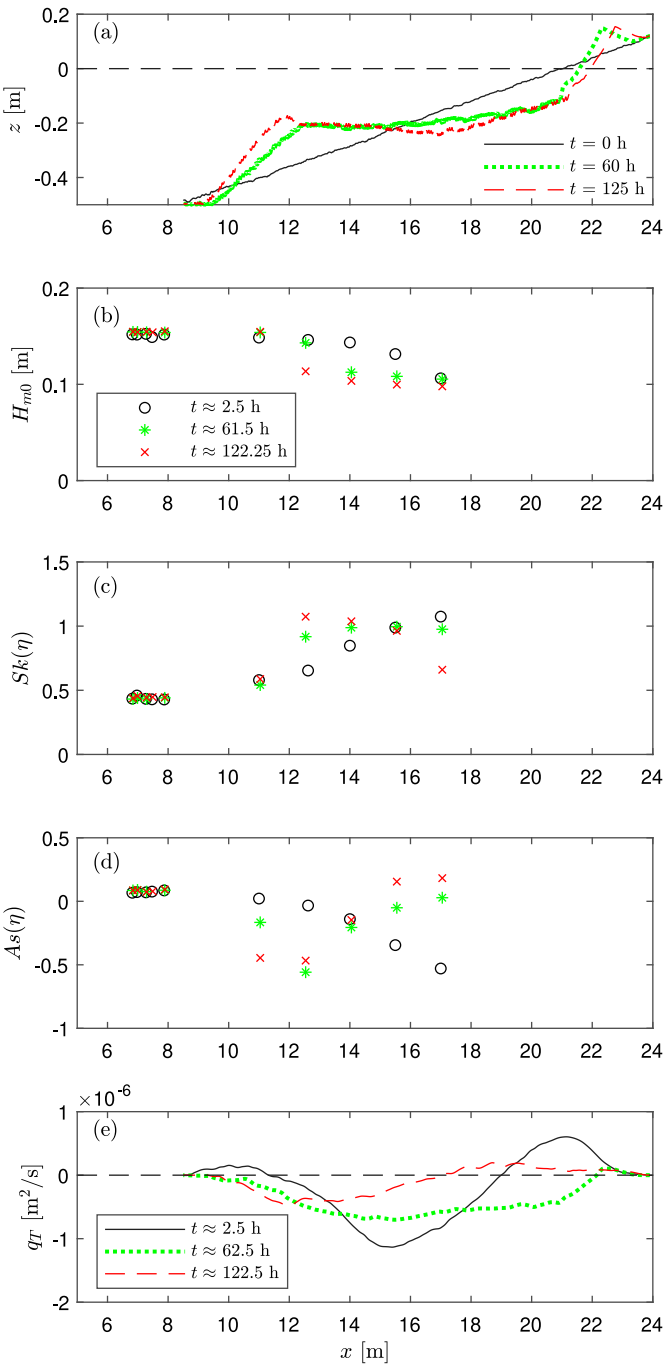

Fig. 5. (a) profile development, (b) characteristic wave heights, (c) skewness, (d) asymmetry and (e) transport rates.

the implications for equilibrium profiles will be further discussed in Section 4.

For the present experiments it is very important that there is a high degree of repeatability, such that the nourishment cases can be compared to each other and to the reference (un-nourished) case. Fig. 6 shows the reference case and the reshaped bed profiles at $t = 25$ h and $t = 60$ h (Fig. 6a,b), as well as the profiles after an additional 15 h of waves (Fig. 6c,d). Fig. 6e,f show the difference in the profiles between the two moments in time and the corresponding sediment transport rates are shown in Fig. 6g,h. The characteristic wave heights, skewness and asymmetry are shown in Fig. 6i–n. Overall the figure indicates excellent agreement between the reshaped profiles and the reference

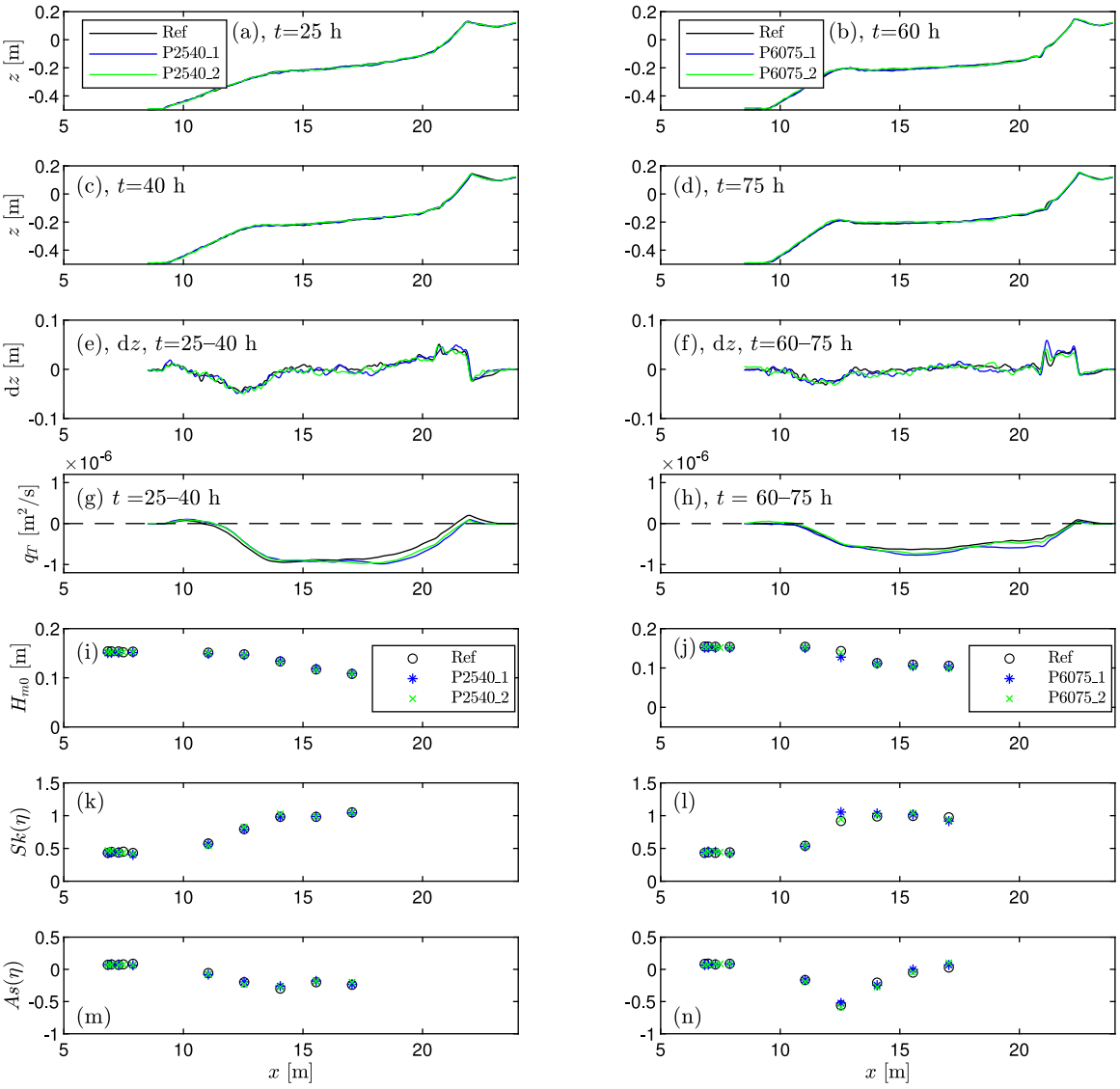

Fig. 6. Profiles of the reference case and the reshaped cases at (a) $t = 25$ h, (b) $t = 60$ h, (c) $t = 40$ h, (d) $t = 75$ h, changes in bed profiles from (e) $t = 25$–40 h and (f) $t = 60$–75 h and characteristic wave heights, skewness and asymmetry at these time (i-n).

case. Fig. 6a,b shows that the profiles can be reshaped accurately and Fig. 6c,d shows that the morphology following an additional 15 h of waves is also very similar. This can be seen even more clearly by focusing on the difference between the profiles 6e,f and the associated sediment transport rate shown in Fig. 6g,h. Finally, Fig. 6i–n, show that the characteristic wave height, skewness and asymmetry are also very well reproduced, as could be expected based on similarity in the morphology.

Based on the high degree of repeatability of the morphology and wave parameters shown in Fig. 6 the results of both the reference case and the nourishment cases (initiated with a re-shaped profile) can be justifiably compared with each other.

3.2. Nourishment scenarios

Fig. 7 shows a comparison of the morphological development of the reference case and the four different nourishment scenarios at the same time, with Fig. 7a showing case B40, Fig. 7b showing case T40, Fig. 7c showing case B75 and Fig. 7d showing case T75. All four nourishment cases show behaviour similar to the reference case, with the breaker bar moving in the offshore direction and continuous erosion of the shoreline. In all nourishment cases, the shoreline did not retreat as much as in the reference case (difference between solid black and red lines), and therefore the nourishments clearly had an effect on the shoreline position. The nourishment was, however, not able to stop the erosion, but merely slowed it down. In both bar nourishment cases (Fig. 7a,c) the bar ended up further offshore compared to the reference case, but with a slope and water depth at the bar crest similar to that of the reference case. For the two cases involving nourishment of the trough (Fig. 7b,d), on the other hand, the bar ended up in an almost identical position to the reference case. Most of the nourishment remained in the trough region, with the nourished sand just slightly dispersed compared to the initial placement.

While Fig. 7 compared the nourishment scenarios with the un-nourished reference case, Figs. 8 and 9 compares the different nourishment scenarios to each other in terms of nourishment timing and placement. Fig. 8 compares the effect of the nourishment timing by directly comparing the two trough nourishments (cases T40 and T75, Fig. 8a,c) and the two bar nourishments (cases B40 and B75, Fig. 8b,d). For the trough nourishment cases at $t = 75$ h (Fig. 8a), case T40 has had 35 h of wave action following the nourishment and case T75 has just been nourished. At this time the profiles are distinctly different. In case T40 the beach has been protected and has not eroded as much as in case T75, and in the surf zone the trough nourishment of case

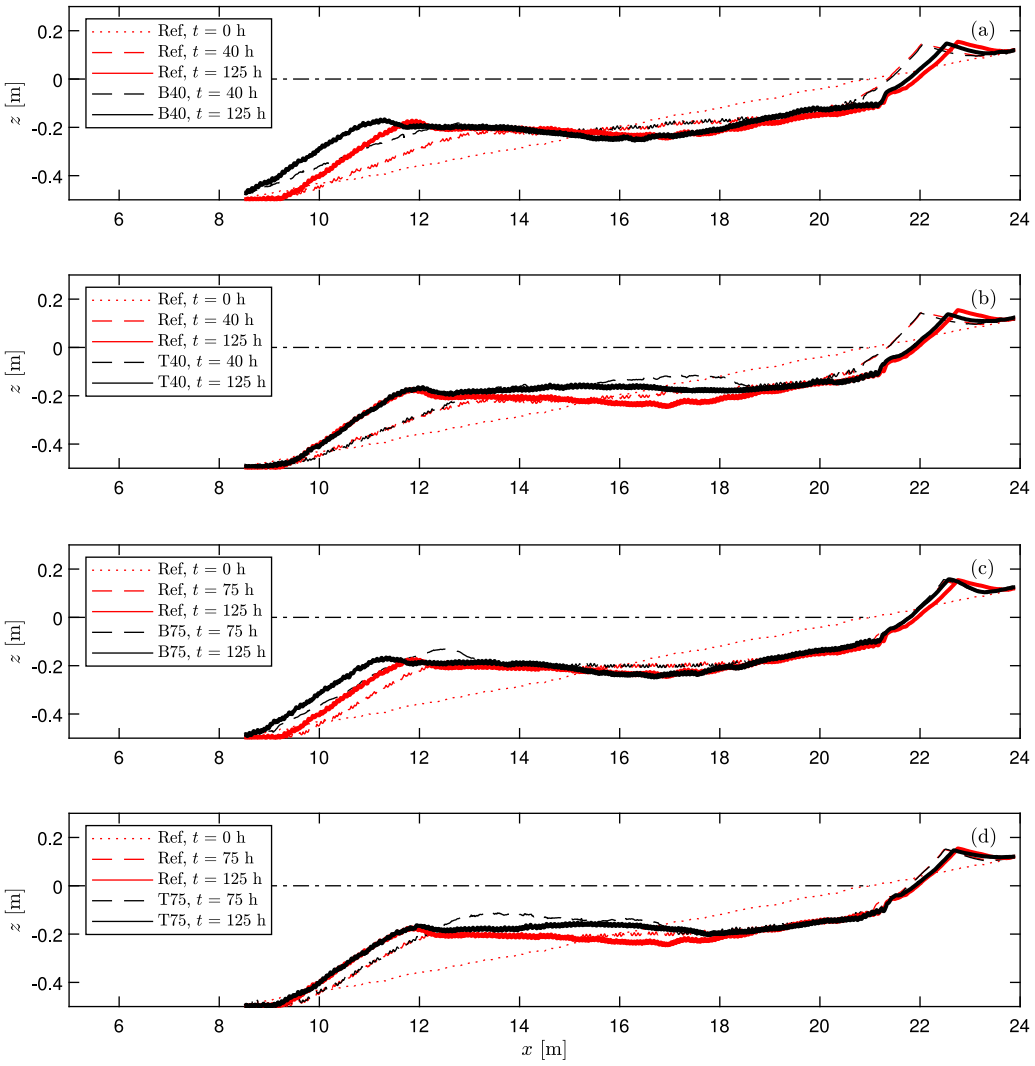

Fig. 7. Comparison of the morphology of the reference case with cases (a) B40, (b) T40, (c) B75 and (d) T75.

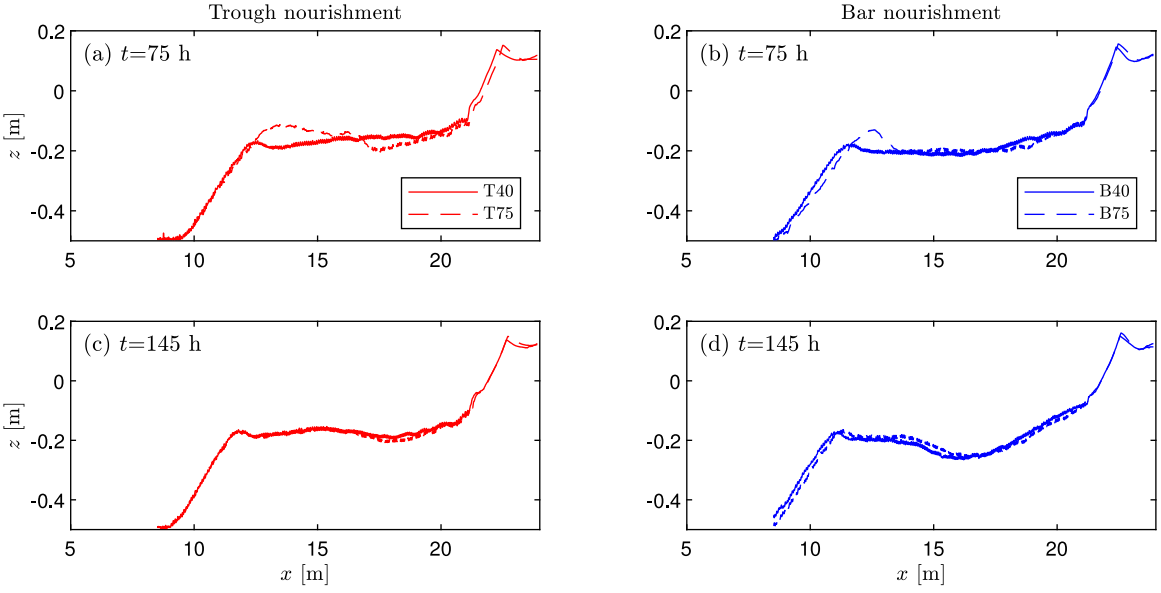

Fig. 8. Comparison of the effect of the timing of the nourishment.

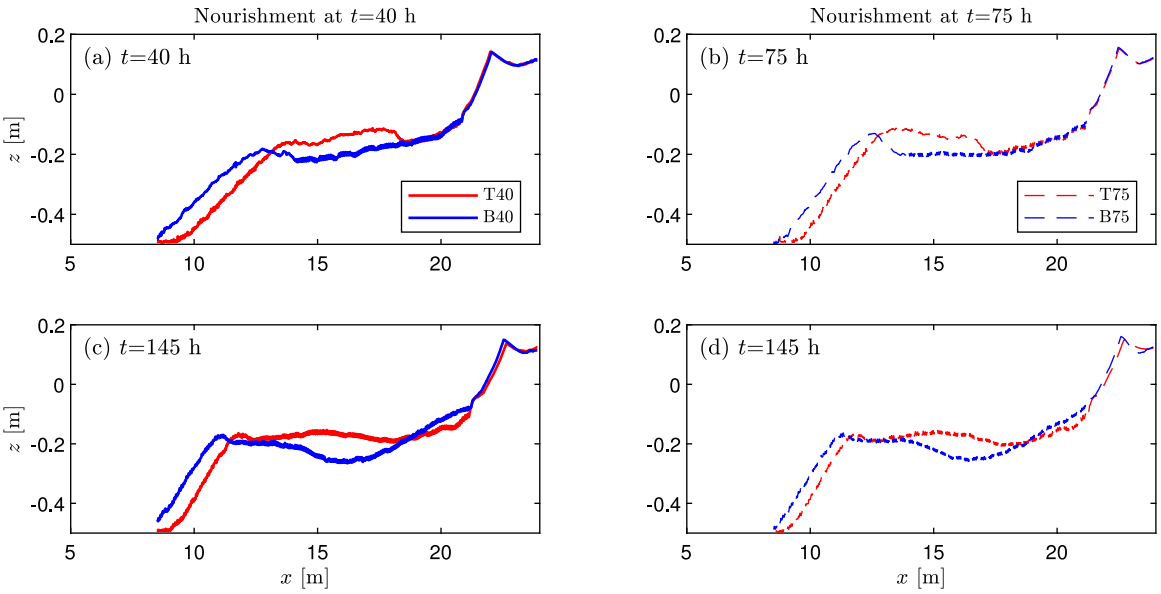

Fig. 9. Comparison of the effect of nourishment strategy.

T75 has resulted in a larger bar compared to case T40. Despite these differences at this time, cases T40 and T75 also have some similarities. The offshore slope of the breaker bar starts at the same location and the slopes of the breaker and beach are also very similar. At $t = 145$ h (Fig. 8c) the profiles of cases T40 and T75 can hardly be distinguished from each other. The main difference is that slightly more sand has been deposited behind the berm in case T75 compared to case T40 and that around $x \approx 18$ m case T75 shows some erosion compared to case T40. This difference is believed to be due to the 35 h of wave action prior to the nourishment, which at $t = 75$ h had moved more sand onshore of the berm (Fig. 8a) and had deepened the region around $x \approx 18$ m. For the bar nourishment cases at $t = 75$ h, case B40 also had 35 h of wave action after being nourished, whereas case B75 has just been nourished. At this time the profiles appear similar, though the offshore slope of the breaker bar is steeper in case B40, and the crest of the breaker bar is less high and positioned further offshore. There is hardly any difference in shoreline position and beach slope, though slightly more sand is positioned onshore of the berm in case B75 compared to case B40, similar to the trough nourishment cases. At $t = 145$ h (Fig. 8d) the profiles appear very similar with only small differences; the breaker bar is positioned slightly further offshore in case B40 compared to case B75, and in the near-shore region ($x \approx 20$ m), case B40 has a slightly shallower depth. The sand in these two regions appears to have come from the surf-zone between $x \approx 11$–15 m. Overall, the large similarity between the profiles in Fig. 8c,d indicates that the timing of the nourishment is not very significant.

Fig. 9 shows the effect of nourishment strategy by directly comparing the trough nourishment cases to the bar nourishment cases. In both Figs. 9a,b the nourishments have just been placed and have not been subjected to any waves yet. For the bar nourishment cases (B40 and B75) the position of the breaker bar slope and crest is further offshore compared to the trough nourishment cases (T40 and T75), but the offshore slope has remained the same. At $t = 145$ h, Fig. 9c,d demonstrate that case B40 as well as B75 still have the breaker bar positioned further offshore and have a much deeper trough/plateau compared to cases T40 and T75. Both cases also show less shoreline erosion compared to the trough nourished cases and they also have more sand deposited in the near-shore region at $x > 17$ m. From Fig. 9 it can therefore be seen that, at least for the duration of these experiments, the placement of the nourishment had a significant effect on the profile shape.

Close inspection of Figs. 7 and 9 shows that the two cases involving nourishment of the bar reduced the shoreline erosion the most. This is shown more clearly in Fig. 10, which compares the shoreline position, horizontal position of the breaker bar crest and the depth at the bar crest in the reference case with the four nourishment cases. For the shoreline position (Fig. 10a), it can be seen that the two trough nourishment cases end up with almost the same shoreline position after 145 h, and similarly the two bar nourishment cases also have almost the same shoreline position after 145 h, i.e. there is little effect of nourishment timing, which also followed from the previous profile comparisons. One case (B40) was continued significantly longer (until $t = 206$ h) and it can be seen that the shoreline actually recovered again. The duration of this case was extended specifically to investigate if the case was truly converging towards an equilibrium, which will be discussed in more detail later on. For now the discussion will focus only on the behaviour until $t = 145$ h. Fig. 10a shows that the shoreline erosion of case T40 is initially slower compared to B40, which follows the reference case closely. The reason for this is that the trough nourishment leads to a decay in wave energy that reaches the shore during this period, which can also be seen in Fig. 11. Since the trough nourishment results in a shallower water depth between $x \approx 13$–18 m a larger percentage of the waves that do not break over the bar will still break in the trough region in this case compared to the reference case and case B40. With time, as the nourishment material is dispersed, fewer waves will break in the trough region due to the larger depth. For the horizontal position of the bar (Fig. 10b) it can be seen that both trough nourishment cases follow the reference case closely, whereas for the two bar nourishments cases the bar quickly migrates in offshore direction and remains positioned further offshore, as shown previously in the cross-shore profiles in Figs. 7–9. Finally Fig. 10c shows, that although the trough nourishments initially result in a slightly shallower water depth at the bar, in time the water depth at the bar for all cases is approximately the same with $h_{bar} \approx 0.17$ m.

The differences in morphology between the various cases will be explained by looking at the wave statistics and the transport rates of the individual cases. Fig. 11 shows characteristic wave height, skewness and asymmetry of all the cases at three different times, and Fig. 12 shows the derived sediment transport rates. At $t \approx 50$ h (Fig. 11a–c) it can be seen that the added nourishment in cases B40 and T40 affected the waves compared to the reference case (note that the timing is indicated as an approximate as the individual wave runs of the different cases were not the same length). The waves of case B40 break

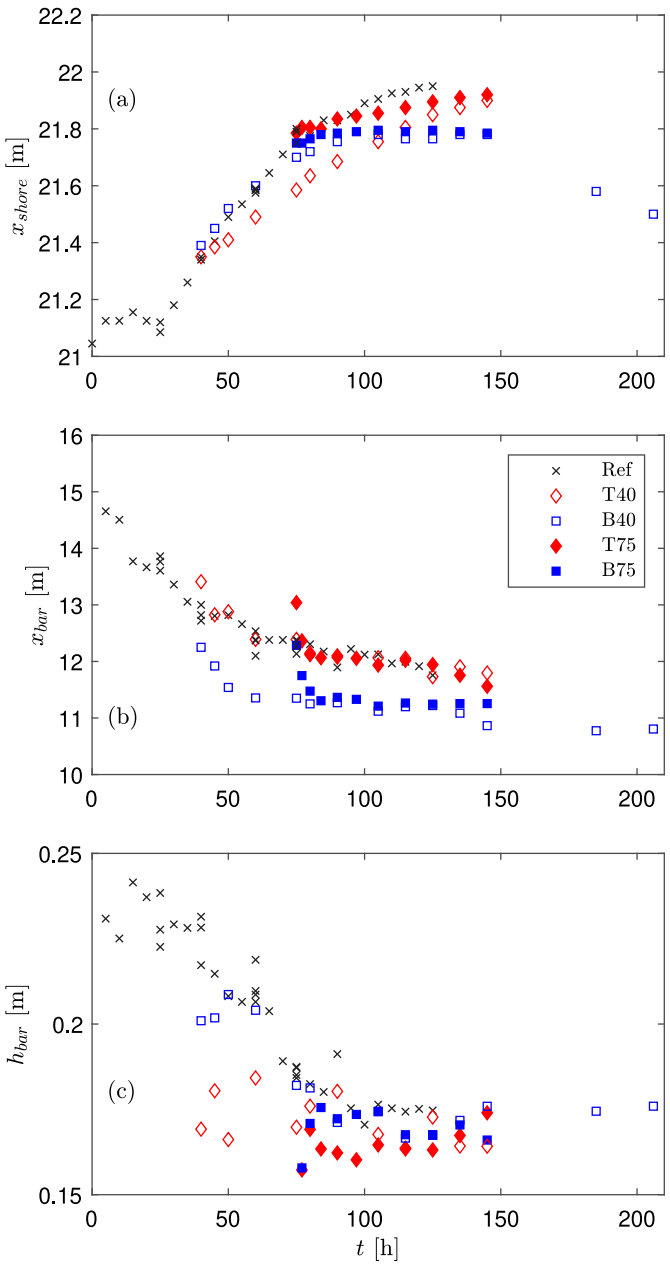

Fig. 10. Comparison between the reference case and the four nourishment scenarios of (a) shoreline position, (b) horizontal position of the breaker bar and (c) water depth at the breaker bar.

earlier (Fig. 11a, blue squares) and have slightly lower characteristic wave heights in the surf zone compared to the reference case. For case T40 (red diamonds), on the other hand, the waves break at the same position as the reference case, but here the added material in the trough causes more waves to break, resulting in lower characteristic wave heights in the inner surf zone ($x > 15$ m), as previously described. For case B40 the skewness and asymmetry (Fig. 11b,c) increase further offshore as a result of the nourishment on the bar slope. In the inner surf zone the skewness even decays a bit in contrast to the reference case, and the magnitude of the asymmetry drops to approximately zero. For case T40 the skewness and asymmetry behave similar to the reference case during shoaling and close to the break point ($x < 13$ m), but further onshore the skewness keeps increasing for case T40, while the skewness for the reference case levels of, and the magnitude of the asymmetry maintains a higher value compared to the reference case. The differences in wave climate for the three cases have implications for the transport rates at this time, which are shown in Fig. 12a. Here it can be seen that the reduced wave energy in the inner surf zone for cases B40 and T40 reduces the offshore directed transport rate, and for case T40 there is almost no net transport in the inner surf zone. This explains the slower shoreline erosion for case T40 compared to case B40 and the reference case as previously seen in Fig. 10a. At $t \approx 80$ h Fig. 11d–f contains now also the wave parameters for cases T75 and B75 (filled markers). Similar to $t \approx 50$ h, it can be seen that characteristic wave heights in the inner surf zone are reduced for all nourishment cases compared to the reference case. The just-nourished case T75 has the greatest reduction of the characteristic wave heights in the inner surf zone, and the just-nourished case B75 has the largest decay in characteristic wave height immediately after breaking. For the wave non-linearities the behaviour is similar to the 40 h nourishments, with the non-linearities of the two bar nourishments reaching a maximum and declining further onshore (Fig. 11e,f, blue symbols), and the two trough nourishments maintaining higher wave non-linearity throughout the surf zone (red symbols). The corresponding sediment transport rates at this time are shown in Fig. 12b. Here it can be seen that the two newly-nourished cases (B75 and T75) show a very similar pattern with the offshore directed sediment transport rate peaking close to the breaker bar, and maintaining an almost zero net flux in the inner surf zone. This is similar to case T40 at $t \approx 50$ h and is probably due to added nourishment resulting in increased wave breaking, which will result in a stronger offshore directed undertow and more sediment in suspension. Both cases B40 and T40 show a cross-shore sediment transport rate pattern similar to that of the reference case, albeit with a slightly reduced offshore magnitude.

At $t \approx 120$ h (Fig. 11g–i) the cross-shore variation in characteristic wave heights is very similar for all cases, though the two trough nourishments result in slightly reduced characteristic wave heights in the inner surf zone. While the characteristic wave heights are very similar, there are still large differences in skewness and asymmetry. For the reference case and the two bar nourishment cases (B40 and B75) the skewness peaks at $x \approx 13$ m and then decays to levels very similar to the incoming waves. The skewness of the two trough nourishments remains high at this time, however. The cross-shore variation of the asymmetry shows the same overall image as the previous time, with the asymmetry increasing in magnitude during shoaling, before declining in the inner surf-zone. Interestingly, at this time the reference case as well as cases B40 and B75 have onshore directed sediment transport shorewards of $x \approx 17$ m. This is in contrast to what might be expected from many process-based explanations, as the undertow in the inner surf zone generally results in offshore directed sediment transport. It should be noted that the increased skewness for the trough nourishment cases could lead to increased offshore directed wave driven sediment transport compared to the bar nourishment cases and the reference case due to unsteady ripple phase lag effects (see e.g. Ribberink et al., 2008; van der A et al., 2013). A possible explanation for the onshore transport is that waves are no longer breaking for $x > 17$ m at this time, which was very visible in the laboratory. For cases T40 and T75 some of the waves also ceased breaking in this region, though some maintained as breakers all the way to the near-shore region. The absence of breaking will result in severely reduced local undertow strengths and turbulence levels in this region. This means that the offshore directed suspended sediment transport will be lower compared to the cases where waves are breaking, and the onshore components of the sediment transport can locally dominate offshore directed cross-shore sediment transport processes (see e.g. Fuhrman et al., 2009, for a description of the processes). The increased cessation of wave breaking for cases B40 and B75 can be explained by the breaker bar being positioned further offshore (waves have to travel further as rollers) and the deeper plateau region with an initial negative slope, which will limit depth-induced breaking and reduce the forward leaning of the waves. Once breaking

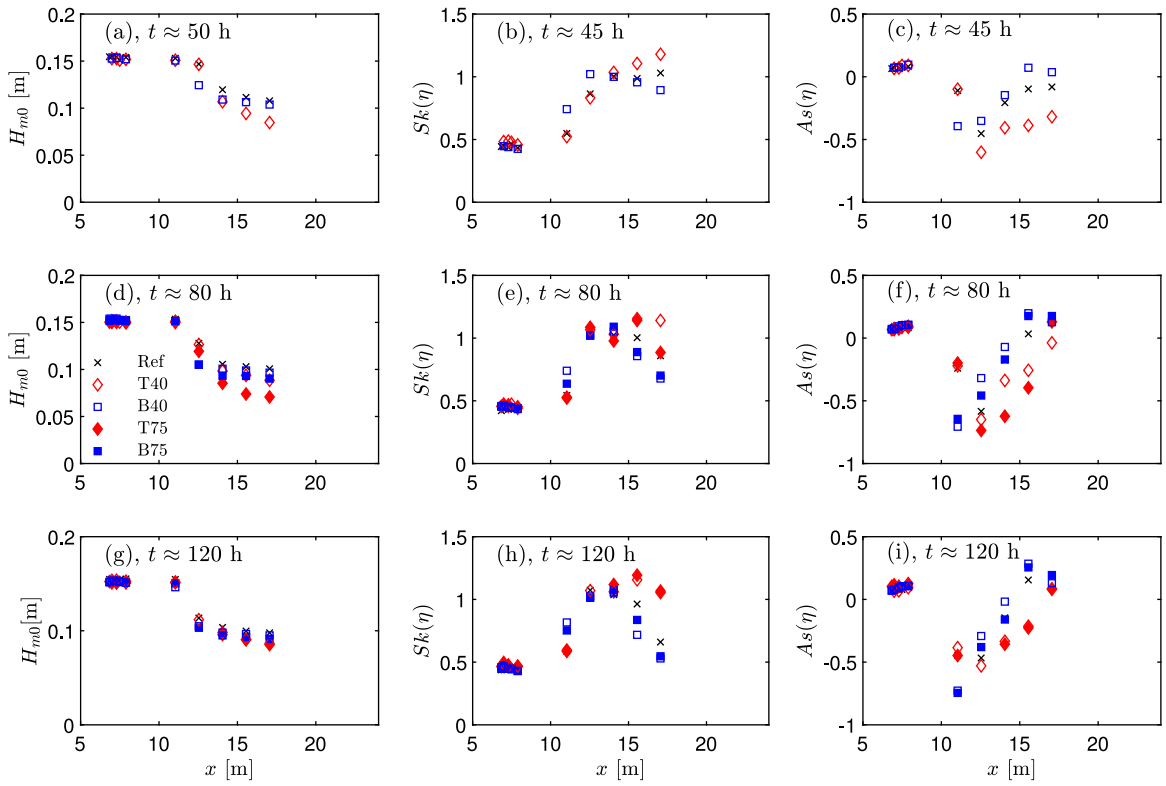

Fig. 11. Comparison of characteristic wave heights (left side), skewness (centre) and asymmetry (right side) at three different times.

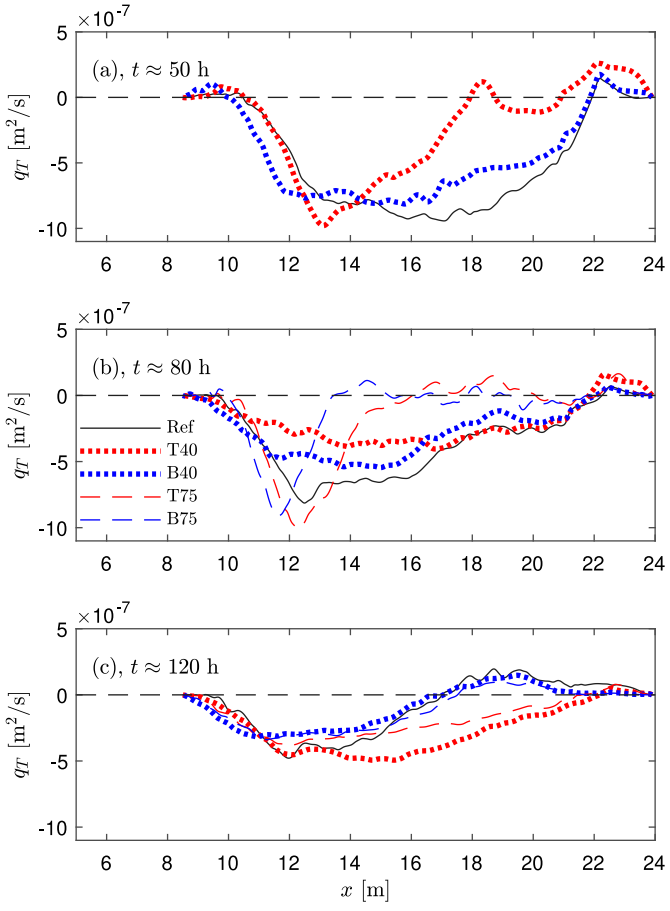

Fig. 12. Transport rates of the five cases at (a) $t \approx 50$ h, (b) ≈ 80 h and (c) ≈ 120 h.

has stopped, the non-breaking waves then shoal and break/collapse a second time very close to the shoreline.

Until the sediment transport rates in the plateau region changed sign in the two bar nourishment cases and the reference case, all cases appeared to have a monotonic development towards equilibrium (see again Fig. 10), which in theory would occur when the net transport rate is zero across the entire profile. After the transport rate changed sign (due to cessation of breaking in the inner surf zone), however, the trend towards equilibrium was disrupted, with sand now returning to the beach. This can be seen in Fig. 13, which shows the profile for case B40 at $t = 145$ h and at $t = 206$ h, as well as the transport rate during this period. Here it can be seen that sand is transported from the region with positive $\mathrm{d}q_T/\mathrm{d}x$ and deposited at the breaker bar region and near the swash zone. Unfortunately this case could not be continued further as all the sand was eroded (down to the underlying fixed slope) in one cross-shore position. Nevertheless, the case shows a clear deviation from a standard monotonic development. At $t = 206$ h it appears that a small bar is forming in the inner surf zone around $x \approx 21$ m, so this profile might eventually have evolved into a two-bar system.

4. Discussion

One of the goals of the present paper is to investigate the importance of nourishment placement and timing for the final shape of coastal profiles. Over the duration of the present experiments, it appeared that timing of the nourishment is relatively insignificant, as the two cases with trough nourishment deployed at different times, ended up with almost identical profile shape. A similar result was found for the two cases where the nourishments were placed along the bar at different times. While the timing of the nourishment seems to be of little importance for the end profile, the choice of nourishment placement affected the end profiles significantly. The sand placed on the offshore side of the bar and on the bar crest reduced the shoreline erosion the most. The bar nourishment caused waves to break earlier compared to the trough nourishments, and at the same time probably resulted

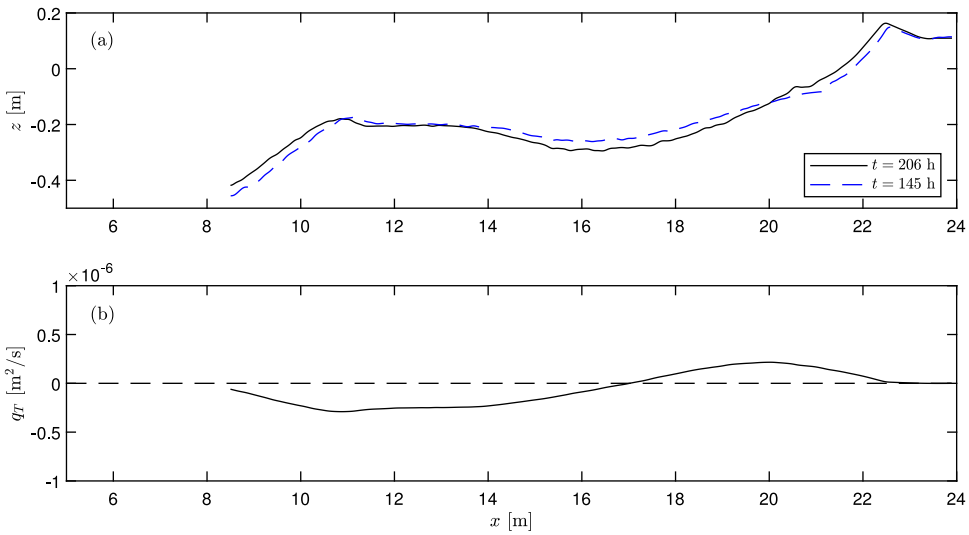

Fig. 13. (a) Bed profiles of case B40 at $t = 145$ h and $t = 206$ h, (b) Transport rate of case B40 from $t = 145$ h to $t = 206$ h.

in reduced undertow strength in the inner surf zone due to the larger water depth in the plateau region. That bar nourishments will always be more efficient than trough nourishments is not a universal finding, however. In the present experiments the transport rate was generally offshore directed, and therefore the nourishment was primarily working as a sheltering mechanism and not a feeder mechanism. Had accretive wave conditions been used following the nourishment, it is very likely that the trough would have been more efficient as the sediment would be closer to the beach.

The nourishments provided shelter in the conventional form, by reducing the amount of wave energy that reaches the coast. An alternative sheltering mechanism was observed towards the end of the experiments, when the breaker bar was positioned further offshore (for the two bar nourishment cases). In this case the wave energy was not reduced as much as in the trough nourishments, but the waves ceased breaking in the plateau region of the inner surf zone, as previously described. A nourishment placed far offshore, creating an artificial breaker bar, could thus be a potential strategy, as also suggested by Jacobsen and Fredsøe (2014). The present experiments indicate that this strategy would especially be efficient if the material is placed far enough offshore so that the waves will not persist (as breakers) all the way to the beach. Such a strategy can potentially backfire though, as the artificial bar can flatten in less energetic conditions and thereby not causing waves to break in subsequent energetic conditions. In this case the nourishment could be completely ineffective.

While the bar nourishment appeared to perform the best over the duration of the experiments, a different conclusion would have been reached if cases B40 and T40 had been stopped after 80 h, in which case the trough nourishment had best protected the beach while the bar nourishment did not have much effect compared to the reference case. The difference in nourishment performance over the shorter and longer time frames within the present experiments can potentially also explain some of the conflicting findings from past nourishment experiments (Walstra et al., 2010; Grasso et al., 2011). These experiments were generally run for significantly shorter duration, and therefore the initial state of the profile will probably have had a large effect on their findings.

In the present study, nourishment placement and timing have been discussed separately. In reality they can be seen as different initial conditions. The question therefore comes down to the following: Does the initial condition matter? Or will the profile always revert to the same equilibrium given a specific forcing and wave climate? The present experiments are inconclusive in this regard, as it was not possible to continue the experiments indefinitely. What can be said, however, is that if such an equilibrium profile exists, the initial condition can play an important role in the time required to reach it. Even in this small scale wave flume setting, after 100 h of morphological time, the cases had still not evolved to an equilibrium profile shape. Others have questioned the presence of a unique static equilibrium given a constant wave forcing and grain size. Baldock et al. (2017) demonstrated that the same Dean number will not necessarily result in the same equilibrium depending on the Dean number of the conditions that created the initial condition. If the initial profile had been created in conditions with a larger Dean number, then the waves were able to pass the breaker bar and continued to erode the shoreline, forming another bar further onshore. They call this "morphological hysteresis". Another example involves cases 2 and 3 from Eagleson et al. (1963) with identical grain size and almost identical wave climates, but with two different initial profile slopes (1/20 and 1/30). After more than 130 h of waves the two profiles both had a breaker bar, but in both cases the initial slope was maintained as the overall profile slope. An effect of the initial condition on the equilibrium can also be inferred from the experiments of Grasso et al. (2009). Their two cases B1 and B2 involving the same sediment and wave climate, but with different initial conditions (B1 was close to a constant slope and B2 had a pronounced bar), ended up with different equilibrium profiles. The profiles had a very similar shape, but with a different profile steepness and several meters difference in shoreline position, which is quite significant in a small scale flume. Grasso et al. (2009) concluded that equilibrium profiles could be achieved, but apparently such profiles are not uniquely determined by grain size and wave conditions. However, recently large scale experiments by Eichentopf et al. (2019), subjected three different initial profiles to the same wave climate and found that the equilibrium profiles were almost identical, contradicting the findings of the present study as well as those from Eagleson et al. (1963), Grasso et al. (2009) and Baldock et al. (2017).

The experiments by Swart (1974) and Atkinson et al. (2018) indicate that a dynamic, rather than static, equilibrium may exist. Atkinson et al. (2018) showed a cyclic bar behaviour under constant wave forcing, with the breaker bar decaying in height, a new breaker bar emerging further onshore, and then propagation of the new breaker bar in the offshore direction. Inner bars have also been observed to appear in energetic wave conditions in the field, if these conditions were preceded by a highly energetic condition moving the bar offshore, and a subsequent mild condition that flattened the bar (Ruessink et al., 2009). Despite running waves for more than 200 h the present experiments did not show cyclic bar behaviour as seen in Atkinson et al. (2018). The present experiments did eventually show a change in sign of the

sediment transport rate in the inner surf zone, and a return of sand to the beach. This was believed to be related to cessation of wave breaking, and thereby the existence of an additional shoaling and breaking region near the coastline. Sand returning to the beach after a long duration also happened in the experiments conducted by Eagleson et al. (1963). In a similar size flume with similar wave conditions, sand started returning to the beach after approximately 100 h of waves (see figure 8 in Eagleson et al., 1963). This behaviour is in contrast to standard simplified models of sandbar shoreline coupling, which would typically predict the shoreline moving onshore when the bar moves offshore and the shoreline moving offshore when the bar moves onshore (see e.g. Yates et al., 2009; van de Lageweg et al., 2013 for a shoreline model and a coupled shoreline-sand bar model, respectively). Cessation of wave breaking can therefore be an important additional physical mechanism to account for in such models. A better handling of the cessation of wave breaking might also be an important aspect to consider in process-based profile models which have difficulties predicting onshore sediment transport accurately (see e.g. van Rijn et al., 2011; Ruessink et al., 2012)

At the end of the present case B40 an inner bar appeared to be forming as a result of the onshore transport and the new breaking region. The inner bar forming mechanism here is therefore different from that observed in the experiment of Atkinson et al. (2018), in which the inner bar was formed due to a decay of the outer bar, allowing waves to pass over the bar without breaking.

5. Conclusions

Four different profile nourishment scenarios have been investigated experimentally along with a reference case without nourishment. The initial constant slope of the reference case was subjected to 125 h of waves. The profile developed into a barred profile with a long flat plateau region and a relatively steeper beach, as expected based on the non-dimensional Dean number. Different instants in the development of the reference case were chosen as initial conditions for subsequent nourishment cases, which were run with the same wave climate to study the effect of nourishment timing and placement in relation to the long-term profile development.

The experiments show that all nourishment cases led to less shoreline erosion compared to the un-nourished reference case, but that the erosion of the beach continued in all cases. The experiments further indicate, that under constant wave forcing, the timing of the nourishment deployment is of little importance, as cases utilizing similar nourishment placement ended up with a similar profile shape regardless of the time of deployment.

It has been shown that coastal profile development can be affected over long time frames depending on where in the profile the nourishment is placed. Nourishment placed along the bar and on the bar crest was most efficient in protecting the shoreline over the duration of the experiments. Due to added complexity and scale effects care should be taken in transferring this finding to the field. That one strategy was more efficient that the other, indicates that initial conditions may effect equilibrium profile shape and that a unique static profile equilibrium shape may not exist for a given fixed wave climate and sediment characteristics.

Finally, for very long duration the shoreline moved offshore for cases involving nourishment of the bar. This is in contrast to the typical monotonic behaviour in time of many simplified shoreline models and is in contrast with standard simplified models of sandbar shoreline coupling. This behaviour was explained from the cessation of wave breaking in the inner surf zone, which created a new shoaling region where the transport rate was onshore directed. This physical mechanism can therefore be important to include in such models.

CRediT authorship contribution statement

Bjarke Eltard Larsen: Conceptualization, Methodology, Software, Validation, Formal analysis, Investigation, Data curation, Writing – original draft, Writing – review & editing, Visualization, Funding acquisition. **Dominic A. van der A:** Conceptialization, Writing review & editing. **Rex Carstensen:** Methodology, Investigation, Data Curation, Resources, Writing – review & editing, Supervision. **Stefan Carstensen:** Methodology, Investigation, Writing review & editing. **David R. Fuhrman:** Conceptualization, Methodology, Writing – review & editing, Supervision, Project administration, Funding acquisition.

Declaration of competing interest

The authors declare the following financial interests/personal relationships which may be considered as potential competing interests: Bjarke Eltard Larsen reports financial support was provided by Independent Research Fund Denmark. David R. Fuhrman reports financial support was provided by Independent Research Fund Denmark. Dominic A. van Der A. reports financial support was provided by Independent Research Fund Denmark.

Data availability

The experimental data can be downloaded from: DOI:10.11583/DTU.16739449.

Acknowledgements

The first, second and last authors gratefully acknowledge financial support from the Independent Research Fund Denmark project SWASH: Simulating WAve Surf-zone Hydrodynamics and sea bed morphology, Grant No. 8022-00137B.

References

Atkinson, A.L., Baldock, T.E., 2020. Laboratory investigation of nourishment options to mitigate sea level rise induced erosion. Coast. Eng. 161, 103769.
Atkinson, A.L., Baldock, T.E., Birrien, F., Callaghan, D.P., Nielsen, P., Beuzen, T., Turner, I.L., Blenkinsopp, C.E., Ranasinghe, R., 2018. Laboratory investigation of the Bruun Rule and beach response to sea level rise. Coast. Eng. 136, 183–202.
Baldock, T.E., Birrien, F., Atkinson, A., Shimamoto, T., Wu, S., Callaghan, D.P., Nielsen, P., 2017. Morphological hysteresis in the evolution of beach profiles under sequences of wave climates - part 1; observations. Coast. Eng. 128, 92–105.
Bayle, P.M., Beuzen, T., Blenkinsopp, C.E., Baldock, T.E., Turner, I.L., 2021. A new approach for scaling beach profile evolution and sediment transport rates in distorted laboratory models. Coast. Eng. 163, 103794.
Bruun, P., 1954. Coast erosion and development of beach profiles, no. 44. United States Army – Corps of Engineers – Beach Erosion Board – Technical Memorandum.
Christensen, D.F., Hughes, M.G., Aagaard, T., 2019. Wave period and grain size controls on short-wave suspended sediment transport under shoaling and breaking waves. J. Geophys. Res. 124, 3124–3142.
Dean, R., 1991. Equilibrium beach profiles: Characteristics and applications. J. Coast. L Res. 7, 53–84.
Dean, R., 2002. Beach Nourishment: Theory and Practise, Vol. 18. World Scientific, p. 399.
Di Risio, M., Lisi, I., Beltrami, G.M., De Girolamo, P., 2010. Physical modeling of the cross-shore short-term evolution of protected and unprotected beach nourishments. Ocean Eng. 37, 777–789.
Dubarbier, B., Castelle, B., Marieu, V., Ruessink, G., 2015. Process-based modeling of cross-shore sandbar behavior. Coast. Eng. 95, 35–50.
Eagleson, P., Glenne, B., Dracup, J., 1963. Equilibrium characteristics of sand beaches. ASCE – Proc. 89, 35–57.
Eichentopf, S., van der Zanden, J., Cáceres, I., Alsina, J.M., 2019. Beach profile evolution towards equilibrium from varying initial morphologies. J. Mar. Sci. Eng. 7, 406.
Elgar, S., Guza, R.T., 1985. Observations of bispectra of shoaling surface gravity waves. J. Fluid Mech. 161, 425–448.
Fredsøe, J., Deigaard, R., 1992. Mechanics of Coastal Sediment Transport. World Scientific, Singapore.
Fuhrman, D.R., Fredsøe, J., Sumer, B.M., 2009. Bed slope effects on turbulent wave boundary layers: 1. Model validation and quantification of rough-turbulent results. J. Geophys. Res. 114, C03024.

Galvin, C.J., 1968. Breaker type classification on three laboratory beaches. J. Geophys. Res. 73, 3651–3659.
Gourlay, M.R., 1968. Beach and Dune erosion. Delft Hydraul. Report, M935/M936.
Grasso, F., Michallet, H., Barthélemy, E., 2011. Experimental simulation of shoreface nourishments under storm events: A morphological, hydrodynamic, and sediment grain size analysis. Coast. Eng. 58, 184–193.
Grasso, F., Michallet, H., Barthélemy, E., Certain, R., 2009. Physical modeling of intermediate cross-shore beach morphology: Transients and equilibrium states. J. Geophys. Res. 114, C09001.
Grunnet, N.M., Ruessink, B.G., 2005. Morphodynamic response of nearshore bars to a shoreface nourishment. Coast. Eng. 52, 119–137.
Huisman, B., Walstra, D.-J., Radermacher, M., de Schipper, M., Ruessink, G., 2019. Observations and modelling of shoreface nourishment behaviour. J. Mar. Sci. Eng..
Jacobsen, N.G., Fredsøe, J., 2014. Cross-shore redistribution of nourished sand near a breaker bar. J. Waterw. Port C-ASCE 140, 125–134.
Ojeda, E., Ruessink, B.G., Guillen, J., 2008. Morphodynamic response of a two-barred beach to a shoreface nourishment. Coast. Eng. 55, 1185–1196.
Ribberink, J.S., van der Werf, J.J., O'Donoghue, T., Hassan, W.N., 2008. Sand motion induced by oscillatory flows: Sheet flow and vortex ripples. J. Turbul. 9, 1–32.
Rosati, J.D., Dean, R.G., Walton, T.L., 2013. The modified Bruun Rule extended for landward transport. Mar. Geol. 340, 71–81.
Ruessink, B.G., Pape, L., Turner, I.L., 2009. Daily to interannual cross-shore sandbar migration: Observations from a multiple sandbar system. Cont. Shelf Res. 29, 1663–1677.
Ruessink, B.G., Ramaekers, G., van Rijn, L.C., 2012. On the parameterization of the free-stream non-linear wave orbital motion in nearshore morphodynamic models. Coast. Eng. 65, 56–63.
Swart, D.H., 1974. Offshore sediment transport and equilibrium beach profiles. (Doctoral Dissertaion). Delft University of Technology, TU Delft.
Ting, F.C.K., Kirby, J.T., 1994. Observation of undertow and turbulence in a laboratory surf zone. Coast. Eng. 24, 51–80.
van de Lageweg, W.I., Bryan, K.R., Coco, G., Ruessink, B.G., 2013. Observations of shoreline-sandbar coupling on an embayed beach. Mar. Geol. 344, 101–114.
van der A, D.A., Ribberink, J.S., van der Werf, J.J., O'Donoghue, T., Buijsrogge, R.H., Kranenburg, W.M., 2013. Practical sand transport formula for non-breaking waves and currents. Coast. Eng. 76, 26–42.
van der A, D.A., van der Zanden, J., O'Donoghue, T., Hurther, D., Caceres, I., McLelland, S.J., Ribberink, J.S., 2017. Large-scale laboratory study of breaking wave hydrodynamics over a fixed bar. J. Geophys. Res. 122, 3287–3310.
van der Zanden, J., van der A, D.A., Hurther, D., Caceres, I., O'Donoghue, T., Ribberink, J.S., 2016. Near-bed hydrodynamics and turbulence below a large-scale plunging breaking wave over a mobile barred bed profile. J. Geophys. Res. 121, 6482–6506.
van der Zanden, J., van der A, D.A., Hurther, D., Caceres, I., O'Donoghue, T., Ribberink, J.S., 2017. Suspended sediment transport around a large-scale laboratory breaker bar. Coast. Eng. 125, 51–69.
van Duin, M.J., Wiersma, N.R., Walstra, D.J., van Rijn, L.C., Stive, M.J., 2004. Nourishing the shoreface: Observations and hindcasting of the Egmond case, The Netherlands. Coast. Eng. 51, 813–837.
van Rijn, L.C., Tonnon, P.K., Walstra, D.J., 2011. Numerical modelling of erosion and accretion of plane sloping beaches at different scales. Coast. Eng. 58, 637–655.
Vellinga, P., 1982. Beach and dune erosion during storm surges. Coast. Eng. 6, 361–387.
Walstra, D.J.R., Hoyng, C.W., Tonnon, P.K., van Rijn, L.C., 2010. Experimental study investigating various shoreface nourishment designs. Proc. Coast. Eng. Conf..
Wright, L., Short, A., 1984. Morphodynamic variability of surf zones and beaches - a synthesis. Mar. Geol. 56, 93–118.
Yates, M.L., Guza, R.T., O'Reilly, W.C., 2009. Equilibrium shoreline response: Observations and modeling. J. Geophys. Res. 114, C09014.